J Therm Spray Tech (2018) 27:179–195
https://doi.org/10.1007/s11666-017-0637-3

PEER REVIEWED

The High-Temperature Wear and Oxidation Behavior of CrC-Based HVOF Coatings

Šárka Houdková[1] · Zdeněk Česánek[2] · Eva Smazalová[2] · František Lukáč[3]

Submitted: 6 June 2017 / in revised form: 18 August 2017 / Published online: 13 September 2017

Abstract Three commercially available chromium carbide-based powders with different kinds of matrix (Cr_3C_2-25%NiCr; Cr_3C_2-25%CoNiCrAlY and Cr_3C_2-50%NiCrMoNb) were deposited by an HVOF JP-5000 spraying gun, evaluated and compared. The influence of heat treatment on the microstructure and properties, as well as the oxidation resistance in a hot steam environment ($p = 24$ MPa; $T = 609$ °C), was evaluated by SEM and XRD with respect to their potential application in the steam power industry. The sliding wear resistance measured at room and elevated ($T = 600$ °C) temperatures according to ASTM G-133. For all three kinds of chromium carbide-based coatings, the precipitation of secondary carbides from the supersaturated matrix was observed during the heat treatment. For Cr_3C_2-25%NiCr coating annealed in hot steam environment as well as for Cr_3C_2-25%CoNiCrAlY coating in both environments, the inner carbide oxidation was recorded. The sliding wear resistance was found equal at room temperature, regardless of the matrix composition and content, while at elevated temperatures, the higher wear was measured, varying in dependence on the matrix composition and content. The chromium carbide-based coating with modified matrix composition Cr_3C_2-50%NiCrMoNb is suitable to replace the Cr_3C_2-25%NiCr coating in a hot steam environment to eliminate the risk of failure caused by inner carbide oxidation.

Keywords ceramic matrix composite · high-temperature oxidation · high-temperature wear · HP/HVOF · power plant

This article is an invited paper selected from presentations at the 2017 International Thermal Spray Conference, held June 7-9, 2017, in Düsseldorf, Germany, that has been expanded from the original presentation.

✉ Šárka Houdková
houdkova@vzuplzen.cz

[1] Research and Testing Institute in Plzeň, s.r.o., Tylova 46, 316 00 Plzeň, Czech Republic

[2] University of West Bohemia, Univerzitní 8, 306 14 Plzeň, Czech Republic

[3] Institute of Plasma Physics of the CAS, Za Slovankou 3, 182 00 Prague, Czech Republic

Introduction

The power generation industry is one of the more challenging from the materials point of view. The most stressed components are exposed to a combination of high temperature, aggressive environment and mechanical load. Only materials with superior properties, such as highly alloyed steels or super alloys, can be used for such applications. The material costs can be reduced by the application of surface protective layers that can also increase the functional properties of coated components. The thermal spray technology, namely high-velocity oxy-fuel (HVOF) spraying, is a suitable technology for applying hard, wear-resistant and oxidation-resistant coatings onto the surface of less noble steels.

Among HVOF-sprayed wear-resistant coatings, applicable in high-temperature environments, the chromium carbide-based hardmetals are considered to be the most effective. The metal alloy coatings, although their high-temperature oxidation resistance can be excellent, do not achieve the wear resistance of chromium carbide-based coatings (Ref 1, 2). Otherwise, highly wear-resistant WC-based coatings cannot be applied, if the temperature increases beyond 350-400 °C, due to the low oxidation resistance of WC (Ref 2).

In the group of chromium carbide-based hardmetal, the Cr_3C_2-25%NiCr coating is the most used. Its microstructure and behavior under various loading conditions were described in detail many times (Ref 3-6). The influence of heat treatment on the Cr_3C_2-25%NiCr microstructure and related changes of mechanical, wear and corrosion properties were also addressed (Ref 7-9). A detailed study of Cr_3C_2-25%NiCr behavior was published by Matthews et al. (Ref 10-19).

Based on the results of the above-mentioned studies, the microstructure of Cr_3C_2-25%NiCr coating can be described. As a feedstock material, the powder consists of Cr_3C_2 carbides and a NiCr matrix. During spraying, part of the carbides phase dissolves into the NiCr matrix. The matrix material then contains a higher amount of C and Cr, resulting in the formation of amorphous or nanocrystalline Ni-based phases responsible for the lowering of matrix toughness. Consequently, the amount of the original Cr_3C_2 carbides decreases, and lower carbides such as Cr, Ni_7C_3 or $Cr_{23}C_6$ can be found in the coating's microstructure. The level of carbide dissolution is mainly dependent on the initial powder properties, such size distribution (Ref 5) and carbide size and their distribution in the matrix (Ref 6), and on the temperature during spraying, hence on the technology used and spraying parameters (Ref 5, 6, 14).

Exposing the coatings to high temperature leads to transformation of the as-sprayed composition to the one similar to the original powder. The transformation is characterized by the precipitation of secondary chromium carbide-based carbides from the supersaturated matrix and the disappearance of amorphous or nanocrystalline phases. The kinetics of the precipitation was recently well described in Ref 19. The higher the temperature of the heat treatment, the faster the transformation is and the coarser the secondary carbides are. At 700 and 900 °C, the transformation was completed in 1 day; at 500 °C, it occurred during 1-5 days. Beyond 5 days of exposition, the carbide development significantly slowed down (Ref 10-12, 15, 19).

The cited influence of heat treatment on the microhardness values is contradictory. While in some studies (Ref 7, 10, 12) an increase in microhardness was observed, a decrease was reported elsewhere (Ref 9), in Ref 19, an increase in microhardness was reported for long-term heat treatment at 500 °C due to the precipitation of small carbide phases, but a decrease in microhardness was observed for heat treatment at 700 and 900 °C. The decrease was related to the reduction of solid solutions strengthening the Ni binder and rapid growth in the size of carbide precipitates. In addition, internal oxidation as a factor affecting the measured microhardness has to be taken into consideration. In Ref 10, the inner oxidation was mentioned in relation to the increase in microhardness of the coating, heat treated in an air atmosphere. On the other hand, the secondary carbide precipitation is generally related to the restoration of matrix toughness (Ref 7-10, 12).

As the microhardness and matrix toughness change due to heat treatment, the wear behavior is also influenced. Matthews (Ref 15-17) reported the positive effect of a skeleton network of secondary carbides on the erosion behavior. In Ref 7, the increase in sliding wear resistance due to the carbide re-precipitation in HVOF-sprayed Cr_3C_2-25%NiCr heat-treated coating is described. In the same study, the negative effect of inner oxidation is mentioned, lowering the coating's inner inter-lamellar adhesion and consequently the wear resistance, in spite of the increase in hardness.

The influence of heat treatment on high- and low-stress abrasion resistance was studied recently (Ref 9). In this study, the complex effect of microstructural changes is well described in relation to different loading conditions. In as-sprayed coatings, the carbide dissolution has led to an increase in matrix hardness accompanied by decrease in its toughness. The following heat treatment, responsible for the restoration of the matrix material from a supersaturated condition, caused an increase in its toughness accompanied by a decrease in hardness. The same microstructural changes resulted in different wear resistances in abrasion test, in dependence on the load condition. Under low-stress abrasion condition, the high hardness of solid-solution hardened matrix of as-sprayed coating was responsible for superior wear resistance, while under high-stress abrasion condition, the supersaturated matrix was prone to brittle fracture and consequently to higher wear. After heat treatment, the decrease in binder hardness was responsible for lower wear resistance under low-stress abrasion condition, while under high-stress abrasion condition, the tougher matrix enables to avoid wear by chipping. The importance of the inter-lamellar cohesion and intra-lamellar adhesion for abrasion wear resistance was also confirmed by Bolelli et al. (Ref 5).

While quite a detailed knowledge of as-sprayed and heat-treated Cr_3C_2-25%NiCr coatings exists, less is known about the microstructure and behavior at high temperatures.

Matthews et al. (Ref 16) studied the high-temperature erosion behavior of Cr_3C_2-NiCr coatings. He pointed out the changes in erosion wear mechanism due to the increase in NiCr matrix ductility at elevated temperatures. With increasing temperature the tendency for localized brittle fracture is reduced, while greater degrees of impact energy are dissipated through localized plastic deformation around the indent. The impact loading on the splat boundaries is reduced, leading to a transition in erosion response from splat based to in-splat microstructure based. However, the increased ductility has a drawback of reduction in hardness and therefore less resistance to penetration.

The published results of Cr_3C_2-25%NiCr high-temperature sliding wear behavior differ in dependence on used testing conditions, coatings deposition technology and also type of initial feedstock. In Ref 20-22, the decrease in wear rate was observed, while in the recent studies of Bolelli et al. (Ref 5, 21), the increase in wear by one order of magnitude compared to the room-temperature values was measured.

The key factor to explain the apparent contradiction is difference in testing temperature. Previous studies (Ref 14, 15, 19) showed that the temperatures higher than 650 °C are necessary for secondary carbide precipitation. In Ref 20-22, the temperature of testing was 700 °C or higher [800 °C in Ref 20], enabling the secondary carbide precipitation during the heating and following testing. The precipitation hardening of the matrix contributed to the coating's wear resistance increases. Simultaneously, at higher temperatures, the oxide layer with high hardness and strong adhesion to the coating surface appeared, also positively influencing the wear as well as lowering the coefficient of friction. On the other hand, in the studies applying 400 °C temperature (Ref 5, 21), the significant increase in wear rate was recorded due to the related to thermal softening on the matrix. At lower temperatures, the secondary carbides precipitation does not take place (Ref 5, 9), as well as the continuous oxide film is not created. Nevertheless, the tribofilm consisting from oxidized wear debris and graphite was observed in the wear track, lowering the coefficient of friction compare to the room-temperature testing. The presence of tribofilm is generally considered to have a positive effect on the COF evolution (Ref 5, 20, 22, 23). The importance of coating's initial microstructure, arising in dependence on the used technology and also initial powder feedstock, was in detail studied (Ref 22). It was shown that the different levels of carbide dissolution in the as-sprayed coating lead to a different wear rates measured not only at room, but also at high (700 °C) temperature.

Considering the high-temperature behavior, oxidation has to be addressed. The oxides scale development in hot (700, resp. 800 °C) air on the surface of Cr3C2-NiCr coating is described in Ref 13.

In Ref 17, the mechanism of inner preferential oxidation of carbides at simulated turbine conditions at 900 °C is proposed. In the case of mechanical loading of surface oxide layer, such as erosion, the various types of cracking or fractures of the oxide layer enable the oxygen to penetrate to coating surface. The boundaries between carbides and matrix can serve as a free path for oxygen to penetrate into the coating. The internal oxidation of carbides then starts along the carbide-matrix boundaries, producing CO. The created CO escapes along the carbide-matrix boundaries, expanding the path for further oxygen access. The reported findings were supported by older studies on several alloy-carbide systems (Ref 24, 25). In studies of Chatha et al. (Ref 8, 26), concentrating namely on the hot corrosion behavior of the Cr3C2-NiCr coatings in aggressive environment, the pre-oxidation of the surface was reported to effectively decrease the corrosion rate. Coatings heat treatment at 1000 °C/1 h resulted in clogging the pores of the coating by rapid formation of oxides at the coatings splat boundaries and within open pores, thereby stopping ingress of corrosive elements toward the substrate. In this work, the possibility of preferential carbide oxidation was not studied, being superimposed by the products of high-temperature corrosion.

The generally accepted conclusion, based on published studies, is that the Cr_3C_2-NiCr coating should withstand both mechanical and thermal loads and is suitable for application up to 800 °C.

But occasionally, the oxidation of chromium carbides in a NiCr matrix was observed in a hot steam environment, which can finally cause detrimental coating failure, as shown in Fig. 1 (Ref 27). In Ref 28, the failure of an HVOF 80/20 Cr_3C_2-NiCr coating, applied on part of a power plat process control ball valve, was also reported. During service, the part underwent combination of mechanical loading, thermal loading and exposition to supercritical steam environment, in irregular cycles. As a cause of the failure, the microstructural changes related to carbide precipitation, in combination with mechanical loading and CTE mismatch between the coating and substrate, were identified. The oxidation was mentioned as one of the factors contributing to the coating degradation.

Compared to Cr_3C_2-25%NiCr, little attention has up to now been paid to chromium carbide-based materials with an alternative matrix such as CoNiCrAlY or NiCrMoNb, which can provide improved corrosion, oxidation or wear resistance.

Picas (Ref 29) studied the tribological properties of as-sprayed and heat-treated HVOF-sprayed Cr_3C_2-CoNiCrAlY. Also here, the precipitation of secondary carbide was observed in the vicinity of the heat treatment. With increasing temperature, the presence and growth of another phase, identified as Cr_2O_3, were recorded not only on the coating surface, but also inside the coating, within the lamellae. The influence of the heat treatment on wear resistance was not clearly demonstrated. Even if the positive effect of good frictional properties of the surface oxide layer was observed, the microcracks that originated during the heat treatment decreased the wear resistance. However, the tribological testing was carried out at room temperature. The high-temperature coating performance is expected to differ from that at room temperature.

As the Cr_3C_2-50%NiCrMoNb spraying powder was introduced into the market recently, only a few references are available concerning its performance. In Ref 30, the microstructure and phase composition of both the original powder and the coating are well described. Two types of chromium-based carbides were observed: the expected

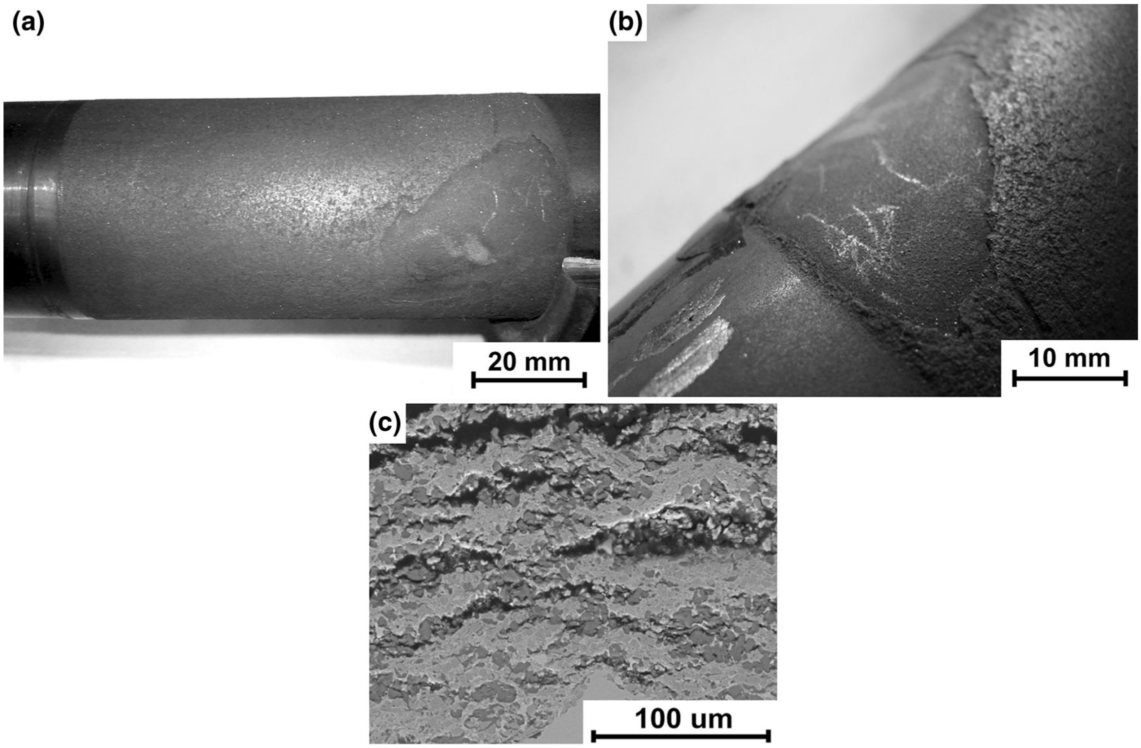

Fig. 1 Detrimental failure of Cr_3C_2-25%NiCr HVOF-sprayed coating working in a hot steam environment: the overview of damaged area (a); detail of the exposed substrate surface (b); SEM of delaminated coating cross section with oxidized carbides (c)

Cr_3C_2 surrounded by a rim of another carbide, supposedly Cr_7C_3. The possible substitution of Cr by Mo and Ni atoms in the lattice of Cr_7C_3 is mentioned, regarding the powder phase composition. Embedded in the Inconel matrix, NbC nano-sized carbides were identified both in the powder and in the coating. The Cr_3C_2-50%NiCrMoNb sliding wear behavior at room and elevated temperatures was further studied and described in Ref 22. Compared to the conventional Cr_3C_2-25%NiCr, the Cr_3C_2-50%NiCrMoNb showed stronger wear; however, the difference was small, considering the difference in matrix content.

The difference was more pronounced during the high-temperature testing. Nevertheless, all the tested chromium carbide-based coating was found to have a great potential as wear resistant at room and elevated temperatures.

The published studies concerning the performance of chromium carbide-based coatings at elevated temperatures are focused namely on the temperatures exceeding 700 °C (Ref 20-22), where precipitation mechanisms already took place, or on the lower temperatures (400 °C) (Ref 5, 21), not sufficient for carbide re-precipitation. In the steam power industry, the working temperatures 580-620 °C arise a question of ongoing microstructural changes and related mechanical behavior. More to that, a little information yet exists concerning the coatings with an alternative matrix.

In Ref 17, the mechanism of inner preferential oxidation of carbides at 900 °C is proposed, but during the oxidation-enhanced erosion test conditions, the emerging protective oxide layer on the surface was continuously removed by erosive particles. The inner preferential oxidation of carbides was not observed in hot air without mechanical loading (Ref 8, 26). The high-pressure hot steam media is more aggressive environment compare to hot air, so further research is necessary to evaluate the oxidation mechanism also for steam power generation working condition.

The aim of this study is to evaluate the microstructural changes, oxidation resistance and wear properties at room and elevated temperatures of chromium carbide-based coating with a typical NiCr matrix and chromium carbide-based coating with highly oxidation-resistant CoNiCrAlY and wear- and corrosion-resistant NiCrMoNb matrices. The oxidation resistance in a hot steam environment was tested to reveal the potential of the coatings to serve in the steam power industry.

Experimental Setup

The thermally sprayed coatings were deposited onto two different substrate materials: carbon steel substrate, used for most of the samples, and high chrome steel for samples tested in the hot steam environment. The sample dimensions were designed according to the requirements of each test: (40 × 30 × 5) mm for microstructure analyses of as-sprayed and hot air-annealed samples, (25 × 25 × 5) mm for the room-temperature (RT) ASTM G-133 test (Linearly Reciprocating Ball-on-Flat Sliding Wear Test), (25.4 × 35.6 × 9) mm for the high-temperature (HT) ASTM G-133 test (Linearly Reciprocating Ball-on-Flat Sliding Wear Test), and cylinder samples (25 mm diameter—25 mm length) for hot steam oxidation tests. Prior to the spraying, the substrates were grit blasted using alumina with 0.8-1 mm grain sizes (F22) to achieve roughness of Ra = 10.4 ± 1.8.

Three commercially available Cr_3C_2-based powders were used to spray the testing samples: Cr_3C_2-25%NiCr (Amperit 588.074), Cr_3C_2-25%CoNiCrAlY (Amperit 594.074) and Cr_3C_2-25%NiCrMoNb (Amperit 595.074). The HP/HVOF TAFA JP5000 spraying device was used. The spraying parameters for each coating are summarized in Table 1. The thicknesses of the sprayed coatings were set to reach 400 µm.

Hot air annealing of the samples was implemented in a muffle furnace (LM 212), at 600 °C for 116 h and cooled in air. The annealing temperature was chosen with respect to the intended coating applications. These components work in the environment of operational steam temperatures in a steam turbine, i.e., 580 °C. The time of the exposure was set to ensure the complete phase transformation in the coating, but simultaneously also to avoid massive surface oxidation. The influence of the duration of exposure on the coating's properties was previously tested (Ref 31). The non-coated parts of steel samples were protected against oxidation by oxidation protective paint CONDURSAL Z 1100.

Hot steam annealing was implemented in the equipment of the laboratory of surface analyses, University of Chemistry and Technology Prague. The equipment enables reaching both the high temperature and pressure of the required atmosphere. For the purposes of this experiment, the testing parameters were set to exceed the expected real working conditions and to accelerate the process of oxidation. The temperature of the autoclave was maintained in the range 608-609 °C; its inside pressure reached 24 MPa. The hot steam environment was prepared from demineralized water with 9.5 pH. For the hot steam oxidation test, the cylindrical samples were ground to reach the surface roughness comparable with real parts surface. The roughness values Ra = 0.21 ± 0.02 for Cr_3C_2-25%NiCr; Ra = 0.3 ± 0.03 for Cr_3C_2-25%CoNiCrAlY and Ra = 0.22 ± 0.01 Cr_3C_2-25%NiCrMoNb were reached.

The as-sprayed and annealed coatings were then analyzed in terms of microstructure, phase composition, microhardness changes and sliding wear behavior.

The microstructure of the coatings was evaluated on cross sections (ground and polished by automatic Leco grinding and polishing equipment) using scanning electron microscope EVO MA25, Zeiss (with LaB6 thermal filament), equipped with EDX detector SDD X-Max 20, Oxford Instruments.

The coatings' phase composition was evaluated and compared by means of x-ray diffraction (XRD), using the D8 Discover powder diffractometer, Bruker, in Bragg-Brentano geometry with a 1D detector and Co$K\alpha$ radiation (scanned region from 15 to 100 °2θ with 0.03 °2θ step size and from 96 s counting time per step). The obtained diffraction patterns were subjected to quantitative Rietveld analysis (Ref 32) performed in TOPAS 5, which uses the so-called fundamental parameters approach (Ref 33). In this manner, (1) the feedstock powder, (2) the surface in the as-sprayed state, (3) the surface of the coating annealed in hot air and (4) the surface annealed in hot steam were analyzed in order to identify the oxides formed in the surface oxide layer together with potential changes of phase composition inside the coatings.

The microhardness was measured on the ground cross sections of as-sprayed and annealed coatings using the HV0.3 method. For each coating, 10 indents were done, and the average value is reported.

The sliding wear resistance and coefficient of friction (COF) were evaluated using the Linearly Reciprocating Ball-on-Flat Sliding Wear test according to ASTM G133. Test parameters were as follows: 25 N Load; steel 100Cr6, 6-mm-diameter ball counterpart; 5-Hz oscillating

Table 1 Coatings deposition parameters

Material	Cr_3C_2-25%NiCr	Cr_3C_2-25%CoNiCrAlY	Cr_3C_2-50%NiCrMoNb
Feedstock	Amperit 588.074	Amperit 594.074	Amperit 595.074
Oxygen	823 l/min	922 l/min	872 l/min
Fuel	25.7 l/h	27 l/h	21.7 l/h
Barrel length	100 mm	150 cm	150 cm
Spray distance	360 mm	420 mm	330 mm
Traverse speed	250 mm/s	250 mm/s	250 mm/s
Feed rate	70 g/min	60 g/min	76 g/min
Carrier gas	Nitrogen, 6 l/min	Nitrogen, 6 l/min	Nitrogen, 6 l/min
Offset	6 mm	6 mm	6 mm

frequency; 10 mm stroke length; 1000 s testing time. The as-sprayed coating was measured at room temperature and at 600 °C. The hot air-annealed samples were measured at room temperature, to evaluate the influence of previous heat treatment on the wear and friction properties.

For each coating, three different measurements were taken. The wear tracks' profiles were measured by the profilometer KLA-Tencor P-6 Profiler, at three different places, and the wear volume was calculated. Prior to the sliding wear tests, the surface of the coatings was ground and polished to the roughness Ra = 0.04 ± 0.02.

Coatings wear resistance was characterized by the coefficient of wear K (mm^3/Nm), calculated from the coating volume loss, used load and sliding distance:

$$K = \frac{V}{L \cdot s},$$

where V is the volume loss (mm^3), L (N) is the load and s (m) is the sliding distance.

After the tests, the SEM of the wear tracks was observed, to identify the wear mechanism.

The roughness of grit-blasted substrate surface and the coated samples was measured by Surftest Mitutoyo SJ-201P, according to DIN EN ISO 4287. The reported values are average from at least ten measurements.

To ensure sufficient adhesion of the coating to the substrate, the adhesion was tested according to ASTM C633. For all the tests provided, the system was broken in a glue. Adhesive/cohesive strength of sprayed coatings exceeds 75 MPa.

Results and Discussion

Microstructure

Feedstock Powder

The feedstock powder's cross sections were analyzed by SEM (Fig. 2) and EDX. The Cr_3C_2-25%NiCr powder (Fig. 2a and b) consists of chromium carbides (1) with cca. 17-19 wt.% of C and 81-83 wt.% of Cr, embedded in the NiCr matrix (2). In the matrix, the significant amount of C (cca. 10 wt.%) was recorded by EDX. Inside the powder particles, a certain amount of porosity is present, and some of the carbides are cracked. The XRD analysis (Fig. 5 and Table 2) does not show the presence of any lower carbides, such as Cr_7C_3, in the feedstock material.

On the contrary, in the cross section of Cr_3C_2-25%CoNiCrAlY powder particle (Fig. 2c and d) three phases were identified: the dark gray phase (3), corresponding to Cr-based carbide, with the measured carbon content between 17 and 20 wt.% and chromium content 79-80 wt.%; the light gray phase (4), consisting mainly of Cr (62-65 wt.%), Co (15-16 wt.%) and C (15 wt.%) with a small amount of Ni (cca 5 wt.%); and the light phase (5), with Ni (60 wt.%) as the dominant element with Co (20-30 wt.%), C (10 wt.%) and Cr (6-10 wt.%).

Correspondingly, the XRD analyses confirmed the presence of both types of carbides, Cr_3C_2 and Cr_7C_3, together with the dominant Ni-based matrix phase (Fig. 7). The results of quantitative Rietveld analyses are summarized in Table 3. Obviously, the measured amount of each phase does not correspond with the nominal powder composition. The total amount of carbides (almost 90 wt.%) exceeds significantly the nominal carbide content (75 wt.%), while the amount of the matrix (11.5 wt.%) is lower than expected at 25 wt.%. With respect to the SEM and EDX observations, the high carbide dissolution during the powder manufacturing process is suggested as an explanation. In area (3), the carbon and chromium content corresponds to the Cr_2C_3, also measured for Cr_3C_2-25%NiCr powder. The light gray phase (4) with a high C content can originate during the manufacturing process from Cr_3C_2 dissolution in the CoNi-based solid solution. This phase corresponds to M_7C_3, where Co and Ni are partly substituting the Cr atoms in the Cr_7C_3 structure. The remaining matrix phase is identified as a Ni-based solid solution.

Compared to Cr_3C_2-25%NiCr, the Cr_3C_2-50%NiCrMoNb (Fig. 2e and f) powder particle cross section is more porous. On the other hand, the carbide cracking is rather limited. The carbide seems to have two different compositions: the dark gray center (6) surrounded by the light gray rim (7). The carbon content varied between 16 and 20 wt.% in the carbide particles. In the light gray rim, the EDX revealed the presence of Mo and Ni, the total amount up to 10 wt.%. This observation is in agreement with those described by Matikainen et al. (Ref 30). In his study, the possible solubility of Mo in Cr_7C_3, substituting the Cr atoms, is mentioned, so rather than Cr_7C_3, the (Cr, Mo, $Ni)_7C_3$ carbide should be referred.

The XRD analyses (Fig. 8) confirmed the presence of both types of carbides, with (Cr, Mo, $Ni)_7C_3$ being dominant (Table 4). The total carbide amount (59 wt.%) exceeds slightly the expected 50 wt.%. Correspondingly, the amount of Ni-based matrix is lower (38 wt.%). In the matrix (8), the high content of C is present (cca 8-11 wt.%), confirming the dissolution of C during powder manufacturing. The discrepancy between the nominal and actual carbide-matrix ratio can be explained, similarly to Cr_3C_2-25%CoNiCrAlY, by the dissolution of the carbides into the matrix material during the powder manufacturing process. Embedded in the matrix, small white precipitates can be found (9), composed mainly of Nb (70 wt.%) and C (cca. 20 wt.%). The XRD method determined the crystal

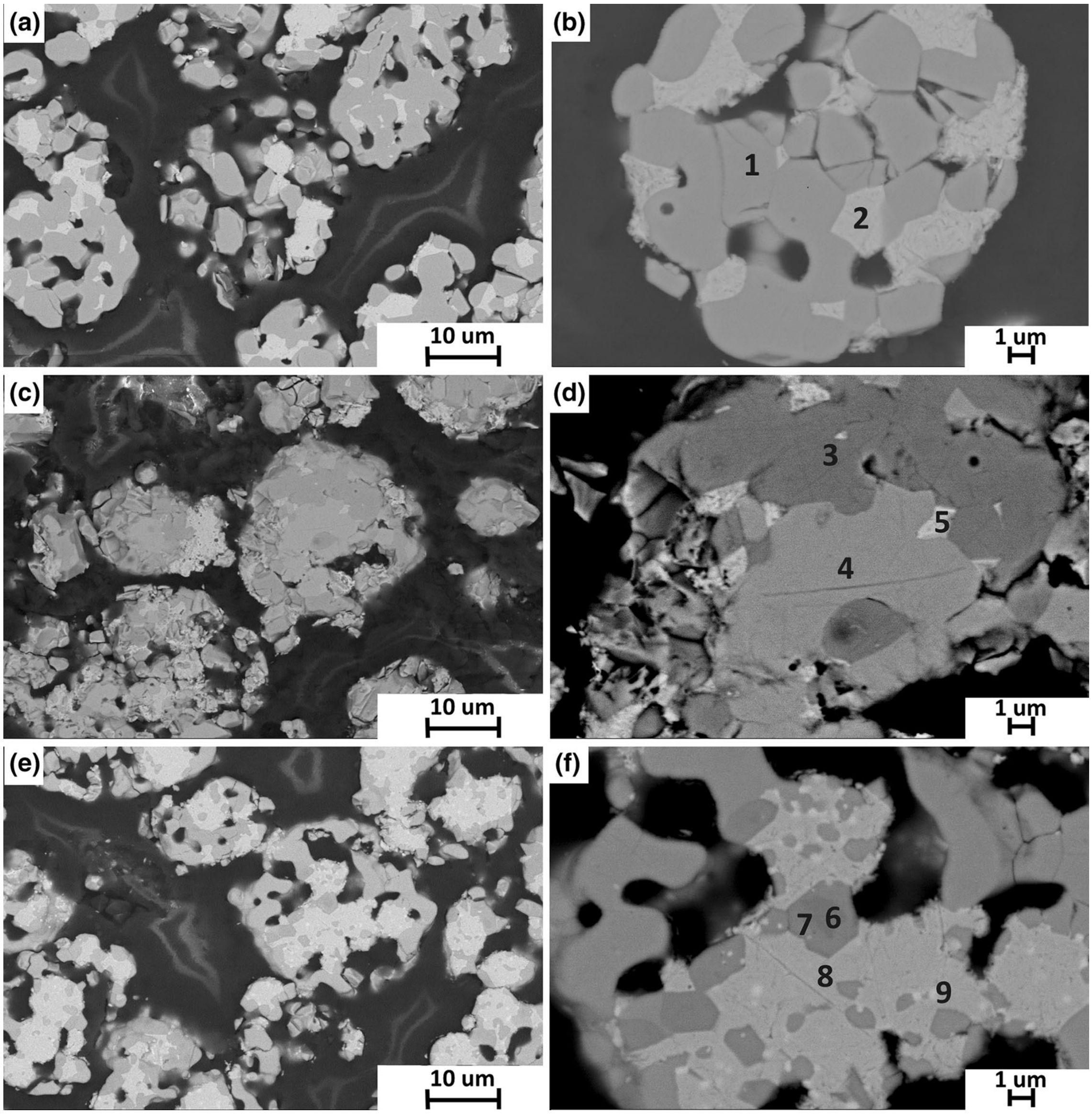

Fig. 2 Microstructure of powder feedstock: Cr_3C_2-25%NiCr (a, b); Cr_3C_2-25%CoNiCrAlY (c, d) and Cr_3C_2-50%NiCrMoNb (e, f)

Table 2 Phase content of Cr_3C_2-25%NiCr coating material in various conditions, based on the Rietveld analysis

Phase composition, %	Cr_3C_2	$(Cr, Ni)_7C_3$	Ni	Cr_2O_3	$NiCr_2O_4$
Powder feedstock	76.5	…	23.5	…	…
As-sprayed coating	26.8	44.7	24	4.5	…
Air-annealed 600 °C/116 h	45.1	…	27.5	27.4	…
Steam-annealed 609 °C/140 h	50.1	…	31.9	16.0	2.0

Table 3 Phase content of Cr_3C_2-25%CoNiCrAlY coating material in various conditions, based on the Rietveld analysis

Phase composition, %	Cr_3C_2	$(Cr, Co, Ni)_7C_3$	Ni	CoNiAl	Cr_2O_3
Powder feedstock	44.6	43.9	9.4	2.1	…
As-sprayed coating	35.6	59.9	1.9	2.6	…
Air-annealed 600 °C/116 h	45.4	12.7	14.5	0.5	26.9
Steam-annealed 609 °C/140 h	29.1	…	17.6	…	53.3

Table 4 Phase content of Cr_3C_2-25%NiCrMoNb coating material in various conditions, based on the Rietveld analysis

Phase composition, %	Cr_3C_2	(Cr, Mo, Ni)$_7C_3$	Ni	Gamma phase	Cr_2O_3	NbC	$NiCr_2O_4$
Powder feedstock	24.5	43.6	30.4	…	…	1.6	…
As-sprayed coating	21.4	31.4	23.0	22.3	0.5	1.6	…
Air-annealed 600 °C/116 h	19.7	19.92	35.2	…	20.9	1	4.4
Steam-annealed 609 °C/140 h	24.8	19.8	43.2	…	10.8		…

structure as being isomorphous with NbC of the FCC cubic space group (No. 225). The NbC presence is also reported in Ref 30.

As-Sprayed Coatings

The microstructure of as-sprayed Cr_2C_3-25%NiCr coating is shown in Fig. 3(a) and (b). Apart from carbides (1), various shades of gray can be seen in the matrix, as a result of carbide dissolution during the spraying process. The darker the gray is, the higher the concentration of C measured by EDX analyses, 20 and 15 wt.% in locations (2) and (3), respectively. The high level of carbide dissolution is confirmed by XRD evaluation. According to quantitative Rietveld analyses, more than half of the carbides transfer from Cr_3C_2 to Cr_7C_3 (Table 2). While only Cr_3C_2 carbides were detected in the original powder, all the transformations occurred during spraying. On the as-sprayed surface, a small amount of oxidation was detected (Fig. 5).

The as-sprayed Cr_3C_2-25%CoNiCrAlY coating (Fig. 3c and d) is highly porous, with poor cohesion. There are numerous cracks and decohesions, namely between the carbides and the surrounding matrix.

The ongoing carbide dissolution during spraying is confirmed by a further increase of M_7C_3 carbide (5) amount accompanied by a decrease of Cr_3C_2 carbide (4) amount and decreased amount of matrix.

The content of each element in the Cr_3C_2, M_7C_3 and Ni-based phases corresponds to those measured in the powder. The carbide dissolution during Cr_3C_2-25%CoNiCrAlY spraying was already reported by Picas (Ref 29).

The Cr_3C_2-50%NiCrMoNb as-sprayed coating (Fig. 3e and f) contains, similarly to the original powder, two types of carbides—the dark gray (7), composed of C and Cr only (Cr_3C_2), and the light gray carbide (8), where Mo and Ni are taking part, probably in (Mo, Ni, Cr)$_7C_3$ already mentioned above. In the surrounding matrix (9), more than 25 wt.% of C is dissolved. The NbC precipitates are embedded in the matrix, similarly to the Cr_3C_2-50%NiCrMoNb original powder. The XRD of as-sprayed coating (Fig. 7 and Table 4) indicates the formation of FCC precipitates with small crystallites and with a bigger lattice parameter in the nickel-based matrix noted as γ-phase.

Air-Annealed Coatings

As expected, the heat treatment has led to a precipitation of secondary carbides from the supersaturated matrix in the microstructure of all three kinds of chromium carbide-based coatings. In the annealed Cr_3C_2-25%NiCr coating's microstructure, no Cr_7C_3 carbides were detected. The phase composition returned to that of the Cr_3C_2 carbides embedded in the NiCr matrix. On the coating's surface, a significant amount of Cr_2O_3 was measured as a result of oxidation in the air atmosphere (Fig. 5 and Table 2). Nevertheless, no sign of inner carbide oxidation was detected (Fig. 4a and b).

The air annealing of Cr_3C_2-25%CoNiCrAlY coating has also led to precipitation of secondary carbides (Fig. 4c and d). Nevertheless, not all M_7C_3 carbides disappeared during the heat treatment, even if its amount was significantly lowered (Fig. 7 and Table 3), while the amount of Cr_3C_2- and Ni-based matrix increased. Similarly, Cr_2O_3 appeared on the surface as a result of oxidation in the air atmosphere. Besides carbide precipitation, inner oxidation was observed (Fig. 4d). The EDX analyses confirmed the high amount of oxygen and chromium in the measured areas (1) and (2). The preferential oxidation of carbides, starting from the carbide-matrix boundary, was previously described by Mathews (Ref 17) for Cr_3C_2-25%NiCr coating working at 900 °C. The inner oxidation of carbides, confirmed by the presence of Cr_2O_3 inside the coating microstructure after the 900 °C heat treatment of Cr_3C_2-25%CoNoCrAlY coating, was also reported by Picas (Ref 29). The high level of porosity in the Cr_3C_2-25%CoNoCrAlY coating, together with many decohesions between carbides and matrix in the as-sprayed coating (Fig. 3d), contributes to the creation of a free path for oxygen, enhancing the inner oxidation even at 600 °C in this study.

In Cr_3C_2-50%NiCrMoNb coating annealed in an air atmosphere (Fig. 4e and f), the precipitation of secondary carbides is the dominant microstructural change as well. Both types of carbides are present: Cr_3C_2 (3) and (Mo, Ni, Cr)$_7C_3$ (4), even if their ratio has changed (Fig. 8 and Table 4). The gamma phase, present in as-sprayed coating, was eliminated by heat treatment. The oxidation of the surface produced mainly Cr_2O_3 oxide, together with a

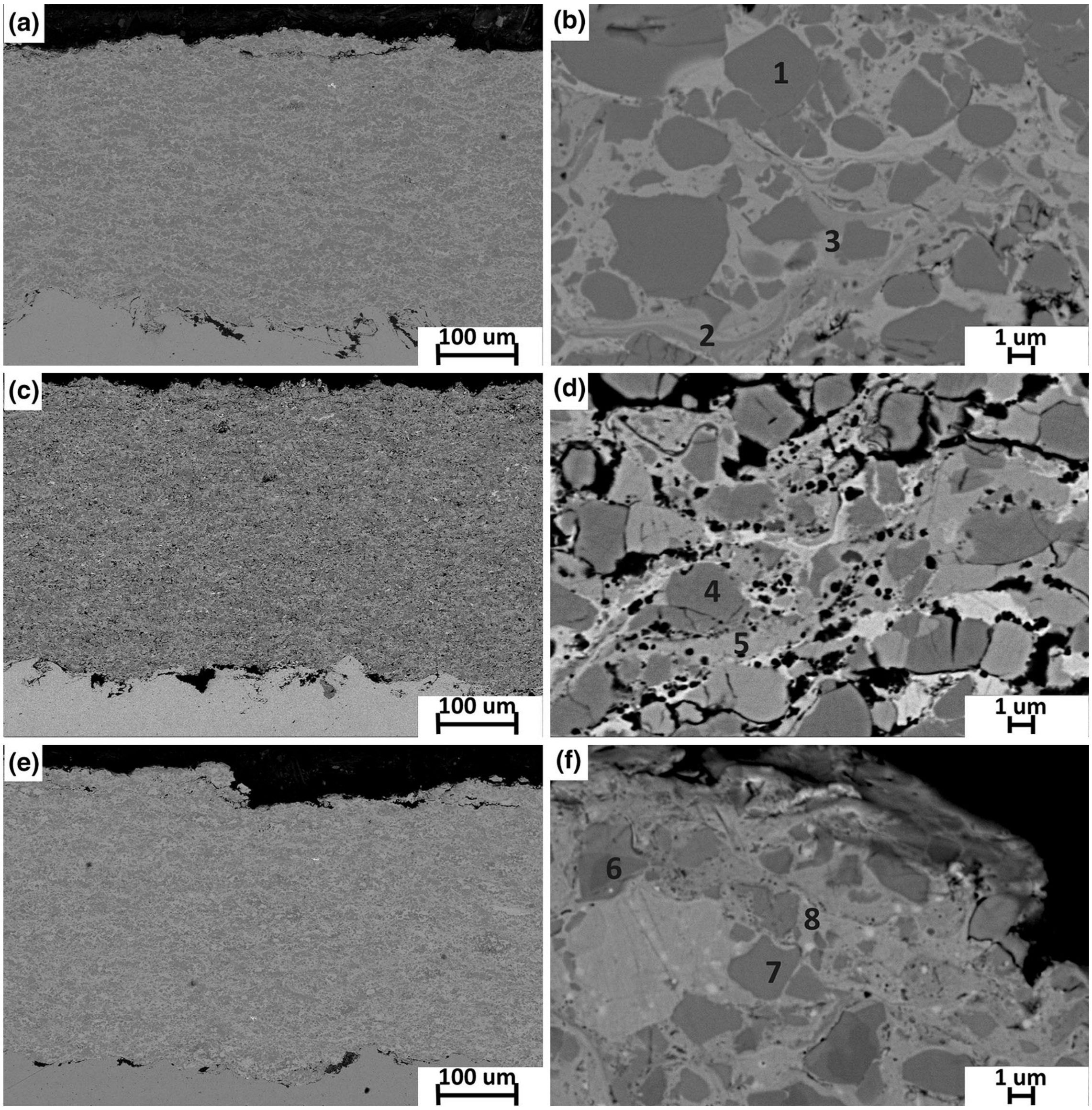

Fig. 3 Microstructure of as-sprayed coatings: Cr_3C_2-25%NiCr (a, b); Cr_3C_2-25%CoNiCrAlY (c, d) and Cr_3C_2-50%NiCrMoNb (e, f)

small amount of $NiCr_2O_4$. No sign of inner oxidation was observed in the coating cross section.

Steam-Annealed Coatings

Secondary carbide precipitation from the supersaturated matrix was observed also in hot steam-annealed coatings' microstructures. The similar temperature conditions and time of annealing led to the carbides' morphologies being similar to those created during annealing in hot air. The change of the environment and increased steam pressure have influenced mainly the amount of oxidation.

The steam-annealed Cr_3C_2-25%NiCr coating's phase composition (Fig. 5 and Table 2) differs slightly from that of the air-annealed. According to quantitative XRD Rietveld analyses, the amount of oxides on the surface is lower. This can be related to the difference in the surface morphology: While the samples for air annealing were left in the as-sprayed state, the samples for steam annealing were ground before the exposition. The higher surface area is responsible for the higher amount of surface oxides. In contrast to air-annealed Cr_3C_2-25%NiCr coating, inner oxidation was recognized in the steam-annealed Cr_3C_2-25%NiCr samples (Fig. 6b). The EDX analyses confirmed the presence of oxygen and chromium in the area (1). The oxidized carbides were found sparsely distributed in the coating close to the surface. Similarly to the air-annealed Cr_3C_2-25%CoNiCrAlY coating, the oxidation starts from the boundary between the carbides and matrix, in agreement with the mechanism proposed by Matthews (Ref 17).

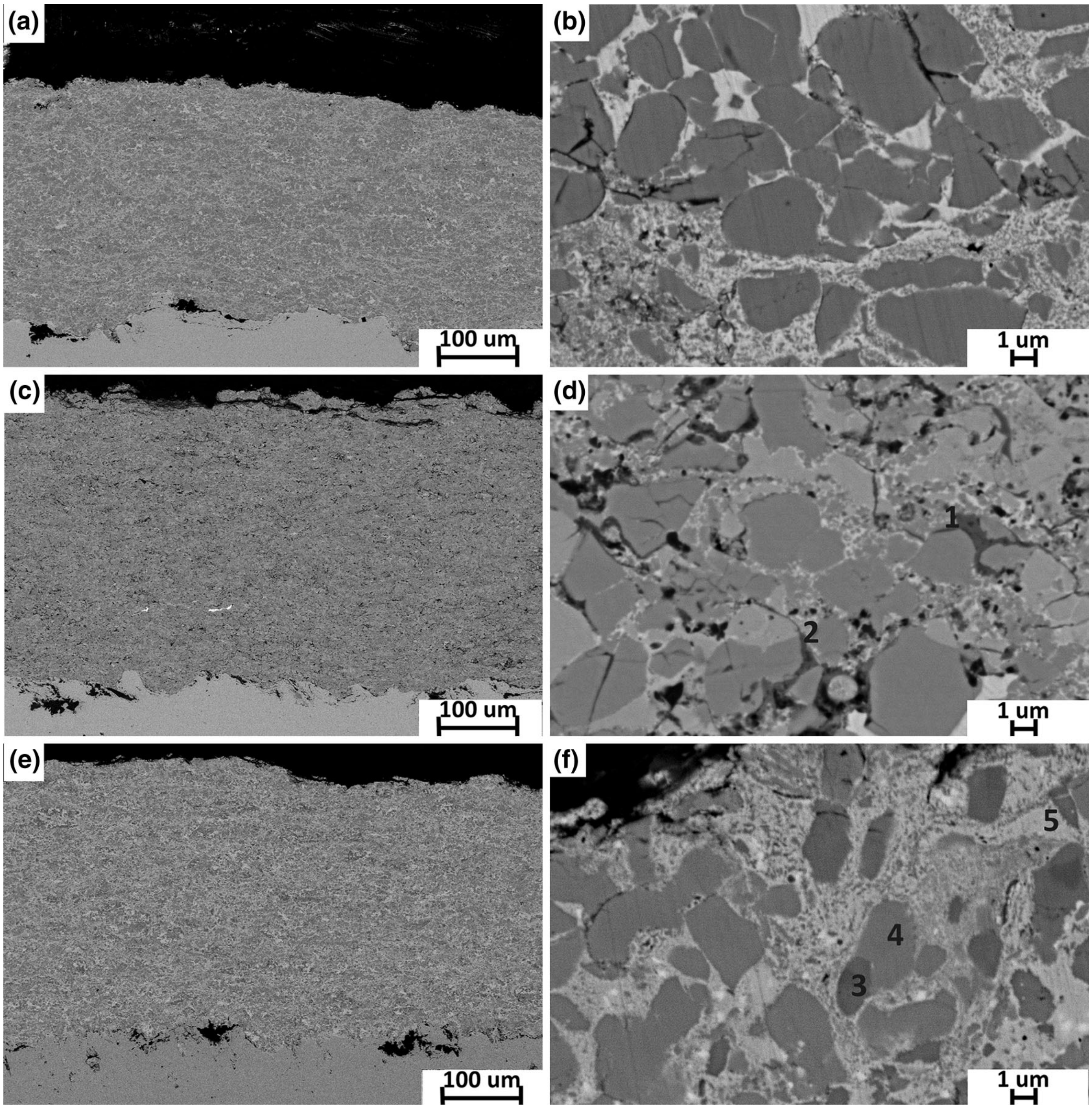

Fig. 4 Microstructure of air-annealed coatings: Cr_3C_2-25%NiCr (a, b); Cr_3C_2-25%CoNiCrAlY (c, d) and Cr_3C_2-50%NiCrMoNb (e, f)

In contrast to moderate subsurface carbide oxidation of steam-annealed Cr_3C_2-25%NiCr coating, massive oxidation of Cr_3C_2-25%CoNiCrAlY occurred (Fig. 6c and d). The coating was destroyed throughout all its thickness. The paths of oxygen spreading into the coating are identified in Fig. 6c. In addition to the porosity and weak boundaries between the carbides and matrix, the boundaries between spraying passes also serve as a path for oxygen to be introduced into the coating and enhance further oxidation. The growing oxide clusters (2) lower the coating's inner cohesion. All the lower carbide Mr_7C_3 was oxidized, together with the majority of regular Cr_2C_3 carbides (Fig. 7). The high level of oxidation is also confirmed by the high amount of Cr_2O_3 detected by quantitative XRD Rietveld analyses (Table 3).

There is no significant difference observed between air- and steam-annealed Cr_3C_2-50%NiCrMoNb coatings (Fig. 4e and f versus Fig. 6e and f). The similar phase composition was confirmed by XRD analyses (Fig. 8 and Table 4). The only difference is the lack of an NbC phase, probably not identified due to its low amount, and the amount of Cr_2O_3 on the surface, higher for the rough as-sprayed surface of the air-annealed sample. The absence of inner oxidation was confirmed by EDX analyses of carbide-matrix boundaries (3) and (4) (Fig. 6f). In both measured places, the content of Cr and C significantly prevails over the amount of oxygen. The dark area was then identified just as decohesion between carbide and matrix.

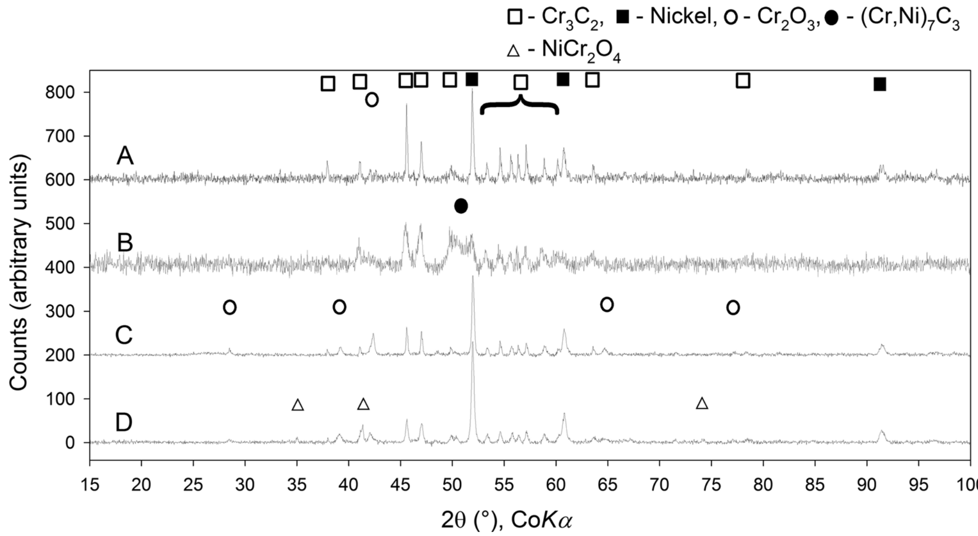

Fig. 5 XRD analyses of Cr_3C_2-25%NiCr: powder (a); as-sprayed coating (b); air-annealed coating (c); steam-annealed coating (d)

Microhardness

To evaluate the changes in mechanical properties in dependence on the annealing procedures, the microhardness HV0.3 was measured on cross sections of the coatings (Fig. 9). In the as-sprayed state, the Cr_3C_2-25%NiCr was the hardest of all three measured chromium carbide-based coatings. After heat treatment, a hardness increase can be observed for the Cr_3C_2-25%NiCr coating. With respect to the typical measurement deviations, there are no differences between air- and steam-annealed samples. In the literature, the microhardness of Cr_3C_2-25%NiCr was reported many times, in the as-sprayed state (Ref 5, 7, 19) and also after heat treatment (Ref 7, 9, 10, 19). The reported HV0.3 values are in agreement with the results measured in this study. In a recent paper by Matthews (Ref 19), a detailed analysis of microhardness evolution in dependence on temperature and time of exposure is presented. For 500 °C, the microhardness increased due to the heat treatment. The increase was related to the precipitation of small carbide grains, responsible for precipitation strengthening. The same mechanism can be proposed also for 600 °C heat treatment.

Contrary to expectation, the hardness of Cr_3C_2-25%CoNiCrAlY is lower compared to Cr_3C_2-25%NiCr. This is caused by the microstructure of the coating, containing a high amount of porosity and decohesions. The annealing procedures increased the microhardness of Cr_3C_2-25%CoNiCrAlY quite significantly. It has to be noted that the indents were located in the areas of the matrix strengthened by secondary carbides, so the influence of oxidation was suppressed. Picas (Ref 29) described Cr_3C_2-25%CoNiCrAlY as having microhardness reaching almost 1050 HV0.3, being further increased by heat treatment up to 1150 HV0.3. In addition to precipitation, oxide development was also mentioned as a reason for the strengthening of the coating. The same trend, an increase in microhardness by heat treatment, was observed also in our study. As the as-sprayed coatings' microstructure contains pores and decohesions, the possibility of splat boundary sintering and reduction of porosity can also play their role in significant microhardness improvement.

The microhardness of Cr_3C_2-50%NiCrMoNb was also lower than that of Cr_3C_2-25%NiCr, but not so dramatically taking into account the higher matrix content. On the other hand, the heat treatment had a low positive effect on its microhardness. Steam-annealed coating even showed a decrease in measured values. The microhardness of Cr_3C_2-50%NiCrMoNb was reported to be 806 HV0.3 in an as-sprayed state and 905 HV0.3 after heat treatment by Matikainen (Ref 22). While the as-sprayed coatings' microhardness value is in agreement with values measured in this study, the strengthening of precipitation was not recorded.

Sliding Wear Behavior

There is just a small difference between the sliding wear resistances of the chromium carbide-based coatings in an as-sprayed state (Fig. 10). The poor microstructure of as-sprayed Cr_3C_2-25%CoNiCrAlY coating does not lead to a significantly higher sliding wear measured at room temperature, compared to Cr_3C_2-25%NiCr. Also, the average wear coefficient value of Cr_3C_2-50%NiCrMoNb is comparable with Cr_3C_2-25%NiCr, despite the higher amount of matrix.

Generally, the measured values are in good agreement with the values reported in the literature: The most often described Cr_3C_2-25%NiCr wear resistance varied from

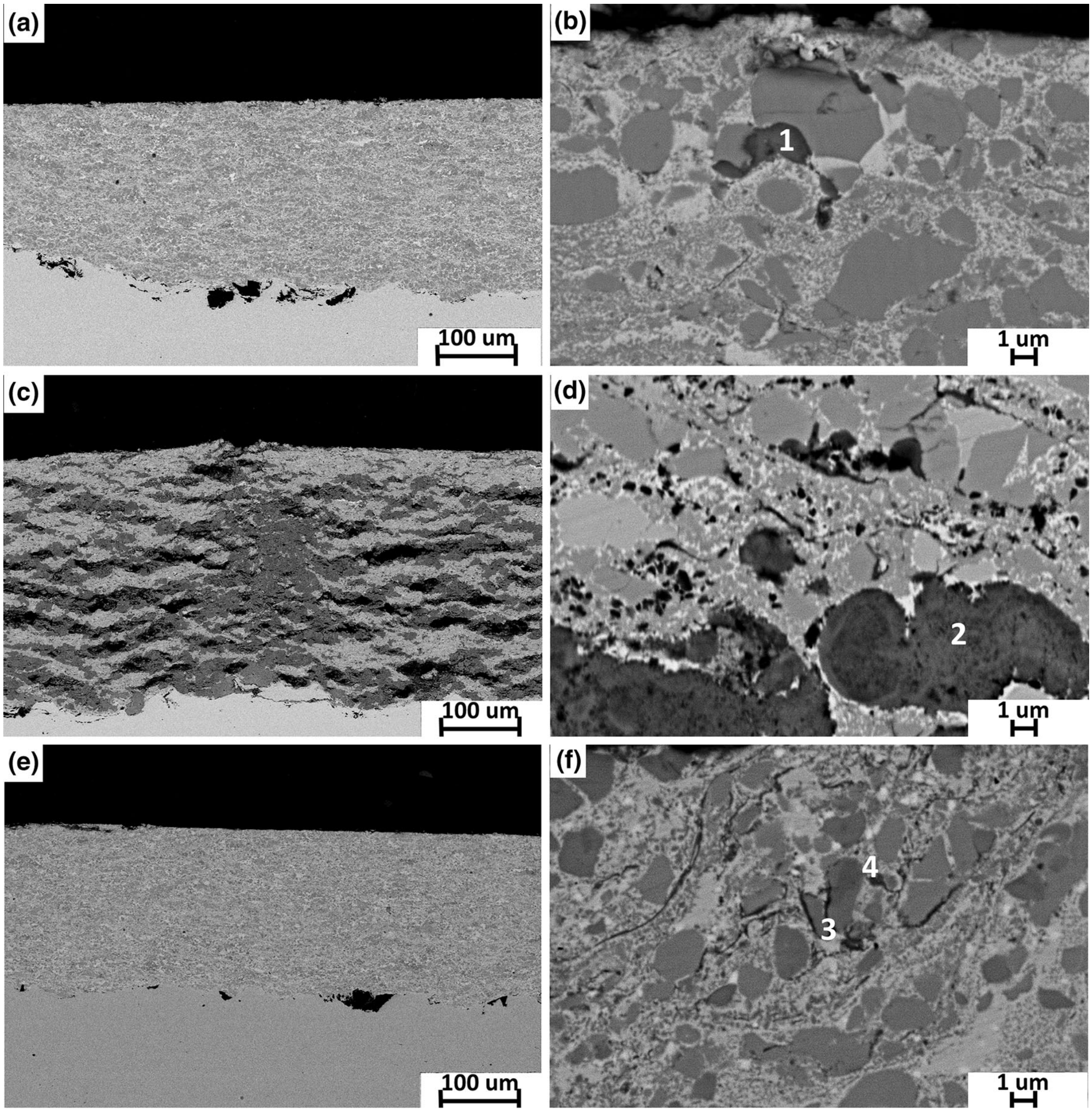

Fig. 6 Microstructure of steam-annealed coatings: Cr_3C_2-25%NiCr (a, b); Cr_3C_2-25%CoNiCrAlY (c, d) and Cr_3C_2-50%NiCrMoNb (e, f)

1×10^{-6} to 1×10^{-5} (Ref 5, 22, 23), the Cr_3C_2-25%CoNiCrAlY reached 7.2×10^{-6} (Ref 29), and Cr_3C_2-50%NiCrMoNb reached 2.2×10^{-6} (Ref 22).

In sliding wear of hardmetals, besides the crucial role of carbide types, sizes and distribution, the matrix material influences the wear mechanism, responsible for wear rate and evolution of COF (Fig. 11).

For Cr_3C_2-25%NiCr coating, the wear mechanism is described in Ref 5 in detail. Generally, three types of wear mechanism take place: (1) abrasive grooving; (2) cracking, fragmentation and pull-out of individual carbide grains; and (3) delamination. The abrasive grooving appears in a consequence of wear debris particles (mostly carbides), trapped between the counterbodies surfaces. The amount of such debris is correlated with the frequency of carbide pull-outs. In carbide pull-out process, the matrix properties, namely the matrix toughness, are important. In the as-sprayed state, the toughness of the matrix is decreased due to the carbide dissolution (Ref 34) and can be more prone to brittle cracking. In Fig. 12(a), the SEM of wear track in the as-sprayed Cr_3C_2-25%NiCr is shown. Both abrasive grooving and the carbide pull-out are marked by arrows in Fig. 12a. The cracking was identified in the wear groove of as-sprayed Cr_3C_2-25%CoNiCrAlY (Fig. 12c). In addition to susceptibility to cracking due to the carbide dissolution, the microstructure of the Cr_3C_2-25%CoNiCrAlY coating did not support the upper-loaded carbides sufficiently due to the high porosity. The cracking was responsible for higher and unsteady friction, especially in the first part of the test (Fig. 11b). Subsequently, tribofilm is created from

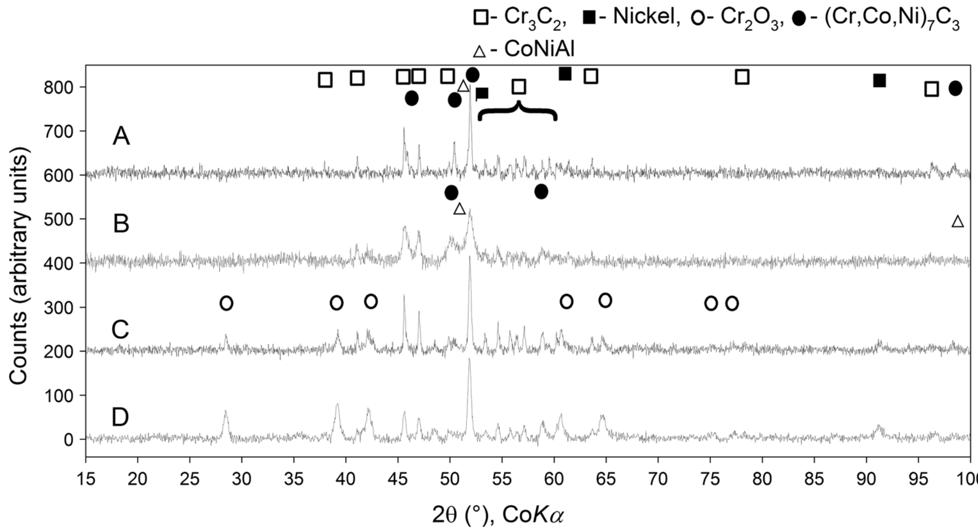

Fig. 7 XRD analyses of Cr_3C_2-25%CoNiCrAlY: powder (a); as-sprayed coating (b); air-annealed coating (c); steam-annealed coating (d)

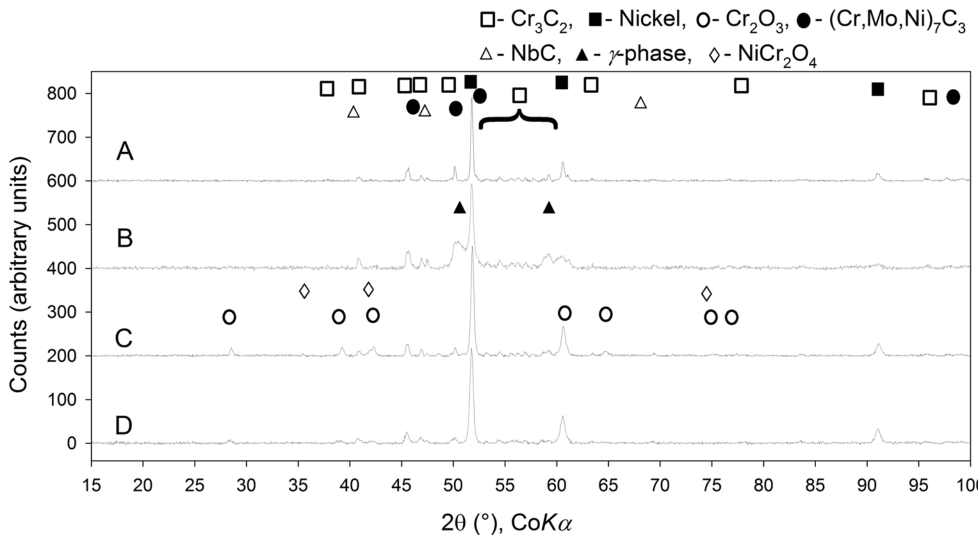

Fig. 8 XRD analyses of Cr_3C_2-50%NiCrMoNb: powder (a); as-sprayed coating (b); air-annealed coating (c); steam-annealed coating (d)

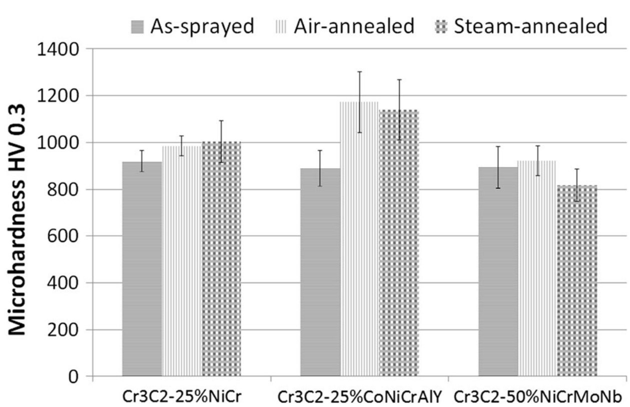

Fig. 9 Average microhardness HV0.3 values with standard deviations

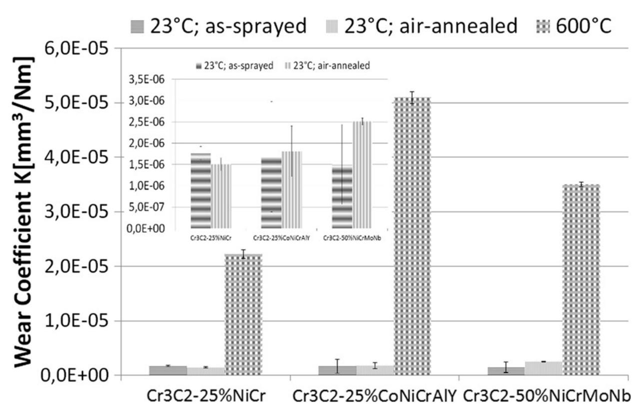

Fig. 10 Sliding wear resistance results with standard deviations

the oxidized debris and transferred counterpart material, leading to a decreased and more stable COF in the second part of the test.

For Cr_3C_2-50%NiCrMoNb, the matrix material and properties are played more important role due to its higher content. The delamination was observed in the wear groove

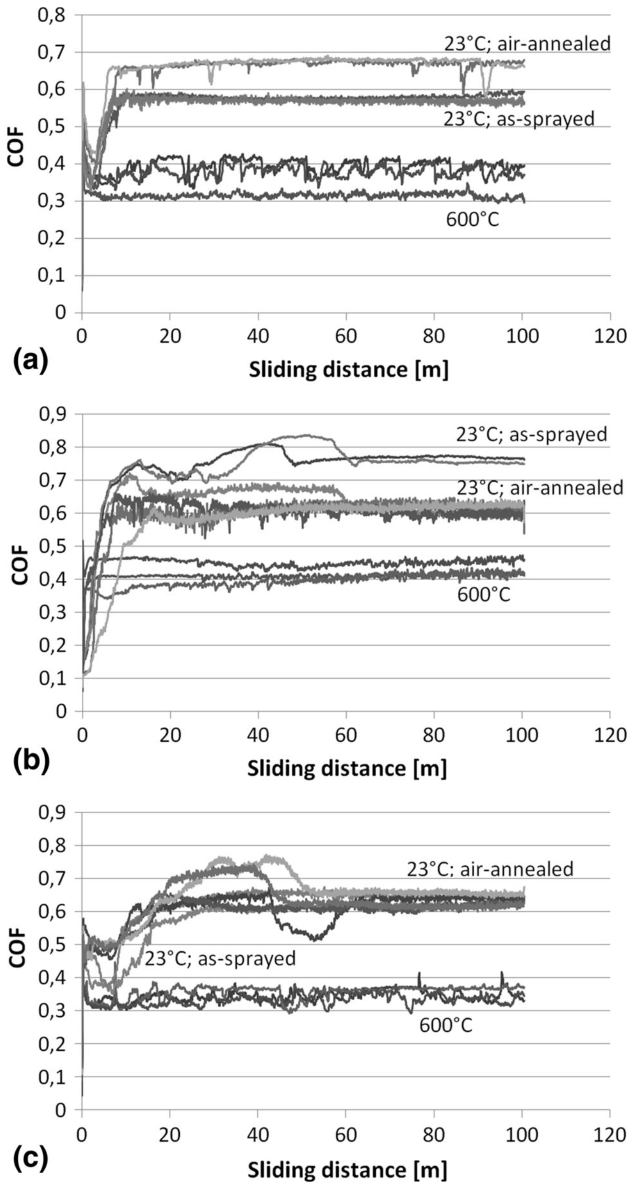

Fig. 11 COF evolution of the coatings tested in different conditions: Cr_3C_2-25%NiCr (a); Cr_3C_2-25%CoNiCrAlY (b); Cr_3C_2-50%NiCr-MoNb (c)

of as-sprayed Cr_3C_2-50%NiCrMoNb coating (Fig. 12e). According to Ref 5, the delamination is connected with the adhesive wear mechanism. Discussing the importance of matrix properties in sliding wear behavior, the presence of gamma phase in the as-sprayed Cr_3C_2-50%NiCrMoNb coating has to be mentioned. The Ni-based superalloys, including Inconel 625, are strengthening by precipitation of intermetallic gamma phases, coherent with the original Ni-based solid-solution structure. Such precipitation strengthening can be achieved by careful heat treatments (Ref 35). The gamma phase, precipitating during spraying process (Fig. 8), together with the presence of fine NbC, dispersed in the Inconel matrix already in the original powder, can be responsible for high wear resistance of Cr_3C_2-50%NiCrMoNb as-sprayed coating, as well as for occurrence of adhesive wear mechanism.

There are several factors to be taken into account when considering the changes of sliding wear resistance as a result of heat treatment, mentioned in the literature (Ref 7, 9, 10, 12, 19). They are including solid-solution hardening of the supersaturated matrix, precipitation hardening connected with heat treatment, the effect of oxidation, which can both increase the hardness, but also decrease the toughness and deteriorate the wear resistance, the sintering of the splat boundary and also changes in the inner stress state caused by annealing.

As the coatings differ in composition and microstructure, the effects of each factor can play their role to a different extent. The Cr_3C_2-25%NiCr coating showed an increase in hardness connected with a decrease in wear. The heat treatment improved its sliding wear behavior through the precipitation hardening mechanism. The higher amount of fine and dispersed carbides contributes to the hardness and wear resistance improvement, together with the restoration of matrix toughness, which is supposed to increase, if the amount of dissolved carbon is decreased. The findings are in agreement with previously published results (Ref 7).

In the case of Cr_3C_2-25%CoNiCrAlY coating, the re-precipitation of fine carbides from the supersaturated matrix was also observed (Fig. 4d), increasing the microhardness and, similarly to Cr_3C_2-25%NiCr coating, contributing positively to the wear resistance. However, the inner oxidation taking place namely on carbide-matrix boundaries (Fig. 4d) plays a negative role (Ref 7). In consequence of this two conflicting effects, the average measured wear resistance value is only slightly higher in comparison with the coating in as-sprayed state, but shows significant typical measurement deviation.

For Cr_3C_2-50%NiCrMoNb coating, the similar positive effect of secondary carbide precipitation effect can be supposed. On the other hand, the higher amount of matrix can play its role. The heat treatment of the coating not only decreased the amount of dissolved carbon, but also eliminated the presence of gamma phase (Fig. 8 and Table 4). The loss of matrix strengthening through gamma phase, together with the inner stress relief of the matrix, can be responsible for matrix with lower resistance to wear. Combining the positive effect of carbide re-precipitation and negative effect of strengthening gamma-phase elimination, the resulted coating wear resistance is lower.

Compared to moderate influence of heat treatment, there is a significant increase in wear, by a degree of magnitude, when testing the coatings at 600 °C. The same was observed during testing at 400 °C by Bolelli (Ref 5).

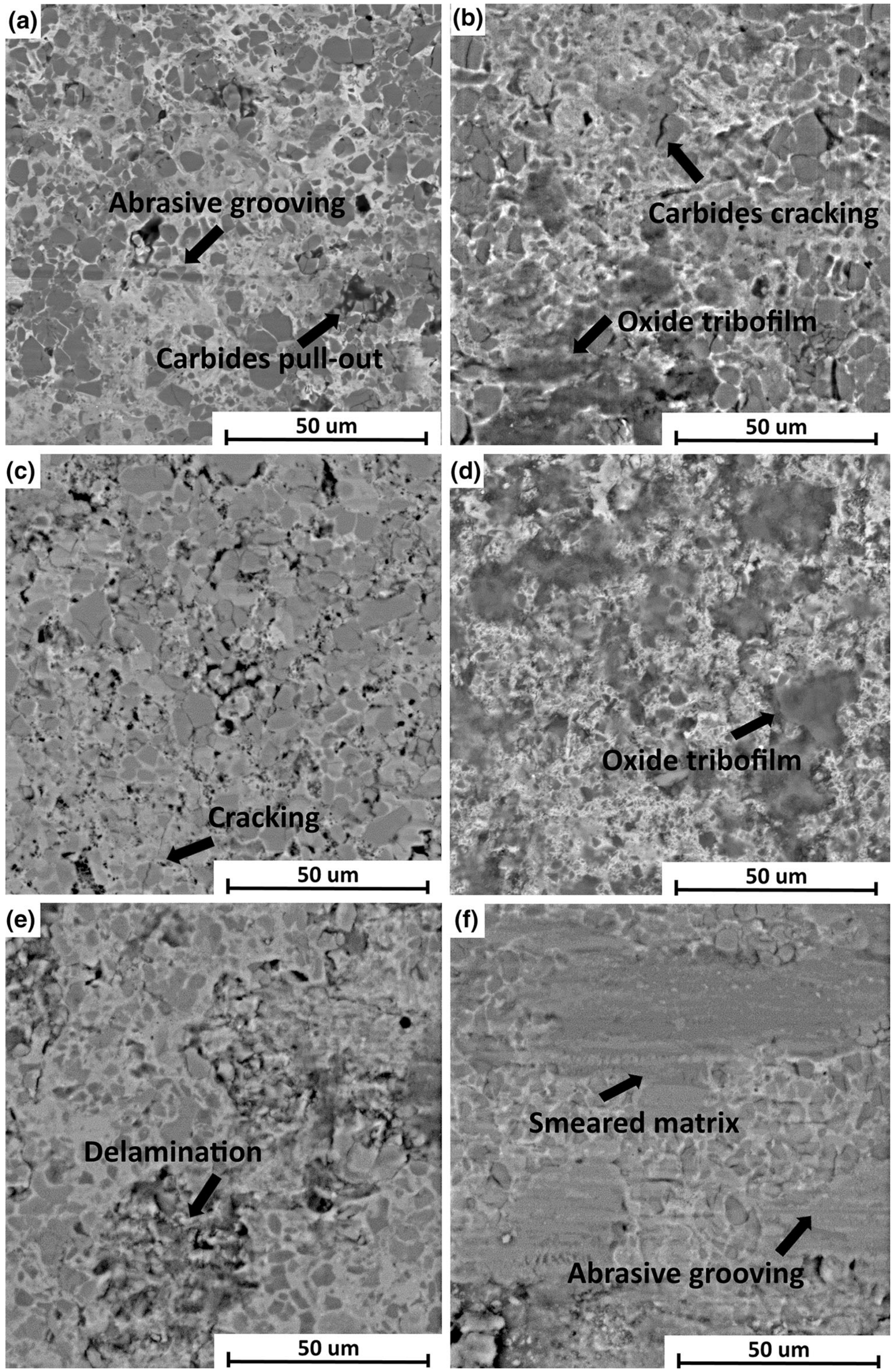

Fig. 12 Sliding wear track of the coatings tested at room temperature and at 600 °C, resp.: Cr_3C_2-25%NiCr (a, b); Cr_3C_2-25%CoNiCrAlY (c, d) and Cr_3C_2-50%NiCrMoNb (e, f)

Matikainen (Ref 22) also observed the increase in the wear rate at 700 °C compare to room-temperature testing; nevertheless, the increase was so significant. Based on the literature review above, the several factors have to be taken into account, considering the high-temperature sliding wear: (1) precipitation of secondary carbides from supersaturated matrix; (2) softening of the matrix material due to the high temperature; (3) creation of continuous and welladhered oxide layer; (4) inner oxidation of chromium carbides during the test.

At 600 °C, the precipitation of secondary carbides was proven for all three evaluated coatings (Fig. 4), so its positive influence on the wear resistance can be assumed, as well as the softening of the matrix material. The matrix can be more easily plastically deformed at elevated temperature (Ref 5), so the abrasive grooving cased by pulled-out carbides is more pronounced. Moreover, the transfer of matrix material on the steel counterpart is more probable at high temperature, increasing the wear rate by adhesive wear mechanism. The matrix-related effect is more pronounced for Cr_3C_2-50%NiCrMoNb coating, due to the higher matrix amount (Fig. 12f). For Cr_3C_2-25%CoNiCrAlY coating, the inner oxidation of carbide-matrix boundaries contribute to the amount of carbide pull-outs (Fig. 12d) and following wear. Together with significant increase in the wear rate, a decrease in COF from 0.6 to 0.8 measured at room temperature to 0.3-0.4 at 600 °C was observed. The decrease in COF can be related to both to softening of the matrix and to the temperature-enhanced creation of the oxide-based tribolayer in the wear tracks. Even if the oxide tribofilm is not continuous (Fig. 12), it decreases the friction significantly.

Conclusion

The chromium carbide-based coating with modified matrix composition Cr_3C_2-50%NiCrMoNb is suitable to replace the Cr_3C_2-25%NiCr coating in a hot steam environment to eliminate the risk of failure caused by inner carbide oxidation. The Cr_3C_2-50%NiCrMoNb coating showed to be the resistant against inner carbide oxidation under the testing conditions. Its wear resistance was found to be comparable with usual Cr_3C_2-25%NiCr at room temperature and have just slightly higher wear at high temperatures.

All three kinds of chromium carbide-based coatings underwent the microstructural changes during the heat treatment in air and high-pressure steam environments at 609 °C. In both environments, the precipitation of secondary carbides from the supersaturated matrix was observed, to an extent depending on the different levels of carbide dissolution in the as-sprayed coating, as well as in the original feedstock powder.

The inner carbide oxidation was confirmed for Cr_3C_2-25%NiCr coating annealed in high-pressure hot steam environment as well as for Cr_3C_2-25%CoNiCrAlY coating in both air and high-pressure hot steam environment.

The microstructural changes of the coatings had a mild effect on the sliding wear, if tested at room temperatures. If tested at 600 °C, the wear of all tree coatings increased, the most significantly for Cr_3C_2-25%CoNiCrAlY in the vicinity of inner carbide oxidation.

Acknowledgment The paper has originated in the framework of the solution of the Technology Agency of the Czech Republic Project Number TE01020068.

References

1. Š. Houdková, F. Zahálka, M. Kašparová, and L.M. Berger, Comparative Study of Thermally Sprayed Coatings Under Different Types of Wear Conditions for Hard Chromium Replacement, *Tribol. Lett.*, 2011, **43**(2), p 139-154
2. L.M. Berger, Application of Hardmetals as Thermal Spray Coatings, *Int. J. Refract. Met. Hard Mater.*, 2015, **49**(1), p 350-364
3. I. Hussainova, J. Pirso, M. Antonov, K. Juhani, and S. Letunovitš, Erosion and Abrasion of Chromium Carbide Based Cermets Produced by Different Methods, *Wear*, 2007, **263**(7-12), p 905-911
4. J.M. Guilemany, J. Nutting, and N. Llorcalsern, Microstructural Examination of HVOF Chromium Carbide Coatings for High-Temperature Applications, *J. Therm. Spray Technol.*, 1996, **5**(4), p 483-489
5. G. Bolelli, L.M. Berger, T. Börner, H. Koivuluoto, V. Matikainen, L. Lusvarghi, C. Lyphout, N. Markocsan, P. Nylén, P. Sassatelli, R. Trache, and P. Vuoristo, Sliding and Abrasive wear Behaviour of HVOF- and HVAF-Sprayed Cr_3C_2-NiCr hardmetal coatings, *Wear*, 2016, **358-359**, p 32-50
6. N. Espallargas, J. Berget, J.M. Guilemany, A.V. Benedetti, and P.H. Suegama, Cr_3C_2-NiCr and WC-Ni Thermal Spray Coatings as Alternatives to Hard Chromium for Erosion-Corrosion Resistance, *Surf. Coatings Technol.*, 2008, **202**(8), p 1405-1417
7. J.M. Guilemany, C. Lorenzana, J. Delgado, J. Sanchez, and C. Martı, Role of Heat Treatments in the Improvement of the Sliding Wear Properties of Cr_3C_2—NiCr Coatings, *Surf. Coat. Technol.*, 2002, **157**, p 207-213
8. S.S. Chatha, H.S. Sidhu, and B.S. Sidhu, The effects of post-treatment on the hot corrosion behavior of the HVOF-sprayed Cr3C2-NiCr coating, *Surf. Coat. Technol.*, 2012, **206**(19-20), p 4212-4224
9. L. Janka, J. Norpoth, R. Trache, and L.M. Berger, Influence of Heat Treatment on the Abrasive Wear Resistance of a Cr_3C_2-NiCr Coating Deposited by an Ethene-Fuelled HVOF Spray Process, *Surf. Coat. Technol.*, 2016, **291**, p 444-451
10. S. Matthews, M. Hyland, and B. James, Microhardness Variation in Relation to Carbide Development in Heat Treated Cr_3C_2-NiCr Thermal Spray Coatings, *Acta Mater.*, 2003, **51**(14), p 4267-4277
11. S. Matthews, M. Hyland, and B. James, Long-Term Carbide Development in High-Velocity Oxygen Fuel/High-Velocity Air Fuel Cr_3C_2-NiCr Coatings Heat Treated at 900 °C, *J. Therm. Spray Technol.*, 2004, **13**(4), p 526-536
12. S.J. Matthews, B.J. James, and M.M. Hyland, Microstructural Influence on Erosion Behaviour of Thermal Spray Coatings, *Mater. Charact.*, 2007, **58**(1), p 59-64
13. S. Matthews, B. James, and M. Hyland, Erosion of Oxide Scales Formed on Cr_3C_2-NiCr Thermal Spray Coatings, *Corros. Sci.*, 2008, **50**(11), p 3087-3094
14. S. Matthews, B. James, and M. Hyland, The Role of Microstructure in the Mechanism of High Velocity Erosion of Cr_3C_2-NiCr Thermal Spray Coatings: part 1—As-Sprayed Coatings, *Surf. Coat. Technol.*, 2009, **203**(8), p 1086-1093

15. S. Matthews, B. James, and M. Hyland, The Role of Microstructure in the Mechanism of High Velocity Erosion of Cr_3C_2-NiCr Thermal Spray Coatings: part 2—Heat Treated Coatings, *Surf. Coat. Technol.*, 2009, **203**(8), p 1094-1100
16. S. Matthews, B. James, and M. Hyland, High Temperature Erosion of Cr_3C_2-NiCr Thermal Spray Coatings—the Role of Phase Microstructure, *Surf. Coat. Technol.*, 2009, **203**(9), p 1144-1153
17. S. Matthews, B. James, and M. Hyland, High Temperature Erosion-Oxidation of Cr_3C_2-NiCr Thermal Spray Coatings Under Simulated Turbine Conditions, *Corros. Sci.*, 2013, **70**, p 203-211
18. S. Matthews, Development of High Carbide Dissolution/Low Carbon Loss Cr_3C_2-NiCr Coatings by Shrouded Plasma Spraying, *Surf. Coat. Technol.*, 2014, **258**, p 886-900
19. S. Matthews and L.M. Berger, Long-Term Compositional/Microstructural Development of Cr3C2-NiCr Coatings at 500, 700 and 900 °C, *Int. J. Refract. Met. Hard Mater.*, 2016, **59**, p 1-18
20. D. Poirier, J. Legoux, and R.S. Lima, Engineering HVOF-sprayed Cr_3C_2-NiCr Coatings: The Effect of Particle Morphology and Spraying Parameters on the Microstructure, Properties, and High Temperature Wear Performance, *J. Therm. Spray Technol.*, 2013, **22**, p 280-289
21. G. Bolelli, B. Bonferroni, J. Laurila, L. Lusvarghi, A. Milanti, K. Niemi, and P. Vuoristo, Micromechanical Properties and Sliding Wear Behaviour of HVOF-Sprayed Fe-Based Alloy Coatings, *Wear*, 2012, **276-277**, p 29-47
22. V. Matikainen, G. Bolelli, H. Koivuluoto, L. Lusvarghi, and P. Vuoristo, Sliding Wear Behaviour of Thermally Sprayed Cr_3C_2-Based Coatings, *Wear* 2017. doi:10.1016/j.wear.2017.04.001.
23. L.M. Berger, M. Woydt, and S. Saaro, Comparison of Self-Mated Hardmetal Coatings Under Dry Sliding Conditions up to 600 °C, *Wear*, 2009, **266**(3-4), p 406-416
24. J.G. Smeggil, The Oxidation Behaviour of an Aligned Co-TaC Eutectic Alloy, *Oxid. Met.*, 1975, **9**, p 225-257
25. F.H. Scott, G.C. Wood, and J.G. Fountain, High Temperature Oxidation of Directionally Solidified Ni-Al-Cr_3C_2 Eutectic, *Oxid. Met.*, 1980, **14**, p 31-45
26. S.S. Chatha, H.S. Sidhu, and B.S. Sidhu, High Temperature Hot Corrosion Behaviour of NiCr and Cr_3C_2-NiCr Coatings on T91 Boiler Steel in an Aggressive Environment at 750 °C, *Surf. Coat. Technol.*, 2012, **206**(19-20), p 3839-3850
27. Š. Houdková and R. Medlín, Analysis of Damage of Thermal Spray Coating Cr_3C_2-25%NiCr, Technical Report No. NTC–VYZ–12–049, New Technology Research Centre, University of West Bohemia, Plzeň, Czech Republic, November 2012 (in Czech).
28. L. Vernhes, D.A. Lee, D. Poirier, D. Li, and J.E. Klemberg-Sapieha, HVOF Coating Case Study for Power Plant Process Control Ball Valve Application, *J. Therm. Spray Technol.*, 2013, **22**(7), p 1184-1192
29. J.A. Picas, M. Punset, S. Menargues, E. Martín, and M.T. Baile, Microstructural and Tribological Studies of as-Sprayed and Heat-Treated HVOF Cr_3C_2-CoNiCrAlY Coatings with a CoNiCrAlY Bond Coat, *Surf. Coat. Technol.*, 2015, **268**, p 317-324
30. V. Matikainen, H. Koivuluoto, and P. Vuoristo, Microstructural Characteristics of Different Cr_3C_2 Coating Compositions Sprayed with HVOF and HVAF Processes *Surface Modification Technologies XXVIII*, ed. T.S.Sudharsan, P. Vuoristo, H. Koivuluoto, June 16-18, 2014, (Tampere, Finland), Valardocs, 2015, p 77-87.
31. Š. Houdková, J. Černý, Z. Pala, and P. Haušild, High Temperature Resistance of Selected HVOF Coatings, *Key Eng. Mater.*, 2015, **662**, p 111-114
32. H.M. Rietveld, A Profile Refinement Method for Nuclear and Magnetic Structures, *J. Appl. Crystallogr.*, 1969, **2**(2), p 65-71
33. R.W. Cheary and A. Coelho, A Fundamental Parameters Approach to X-ray Line-Profile Fitting, *J. Appl. Crystallogr.*, 1992, **25**(2), p 109-121
34. V. Matikainen, G. Bolelli, H. Koivuluoto, M. Honkanen, M. Vippola, L. Lusvarghi, and P. Vuoristo, A Study of Cr_3C_2-Based HVOF and HVAF-Sprayed Coatings: Microstructure and Carbide Retention, *J. Therm. Spray Technol.*, 2017, **26**, p 1239-1256
35. V. Shankar, K.B.S. Rao, and S.L. Mannan, Microstructure and Mechanical Properties of Inconel 625 Superalloy, *J. Nucl. Mater.*, 2001, **288**(2–3), p 222-232